Self-referenced 3D Stress Tensor from NV Centers without a Prior Load Model, Anchored by Diamond Raman

Authors: LFR Resonance Systems Ltd

Date: 2025-11-13

Keywords: NV center, stress tensor, ODMR, diamond Raman, Akahama scale, metrology, provenance

Abstract

Nitrogen–vacancy (NV) centers provide a native vector stress microscope: the hydrostatic ODMR shift and the orientation-dependent splitting jointly encode the full $3\mathrm{D}$ stress tensor. We combine Barson-calibrated NV spin–stress coefficients with an exact Akahama (2010) diamond Raman scale to anchor absolute pressure in GPa. Using multi-orientation ODMR, we least-squares invert the six independent stress components σ without any prior on loading geometry. We validate against uniaxial and hydrostatic curves and show extended cross-axis agreement to $80\ \mathrm{GPa}$, with full artifact provenance ($\mathrm{SHA256}$). This self-referenced, auditable $\mathrm{NV} \leftrightarrow \mathrm{Raman}$ bridge enables wafer-scale, MEMS, and diamond anvil cell (DAC) stress cartography.

---

1. Introduction

- Stress metrology at micro/nano scale benefits from a vector sensor with absolute calibration.
- NV centers in diamond offer orientation-resolved ODMR transitions sensitive to both hydrostatic and deviatoric stress components.
- Prior approaches often assume a load model; here we leverage the multi-orientation response to infer the stress tensor directly from spectra.
- Absolute units come from a paper-accurate diamond Raman calibration by Akahama (2010), providing a robust cross-modal anchor.

---

2. Theory and Equations

2.1 NV hydrostatic and deviatoric response

We adopt Barson (2017) spin–stress coefficients. For hydrostatic pressure P (in GPa), the leading ODMR frequency shift is

$$\Delta f_{\mathrm{hyd}}(P) = a_1 P + 2a_2 P \quad [\mathrm{MHz}],$$

with representative coefficients $a_1 = 4.4 \pm 0.2$ and $a_2 = -3.7 \pm 0.2\ \mathrm{MHz/GPa}$. We denote the ODMR axial shift as $\Delta D \equiv \Delta f_{\mathrm{hyd}}$. Deviatoric components couple via coefficients b, c and generate orientation-dependent splittings across the four $\langle 111 \rangle$ NV sub-ensembles. The predicted frequencies $f_{i,\pm}(\sigma)$ are analytic in the symmetric stress tensor σ.

2.2 Diamond Raman absolute scale (Akahama 2010)

Let ω denote the diamond Raman edge (cm^{-1}). With $\omega_0 = 1334\ \mathrm{cm}^{-1}$ and $x = (\omega - \omega_0)/\omega_0$:

- Standard regime ($\mathrm{Eq.}\ 1$, up to $\sim 200\ \mathrm{GPa}$):

  $$P(\mathrm{GPa}) = Ax + Bx^2, \quad A = 547 \pm 11,\ B = 3.75 \pm 0.20.$$

  Inversion used for $\omega(P)$:

  $$\omega(P) = \omega_0 \left(1 + \frac{-A + \sqrt{A^2 + 4BP}}{2B}\right).$$

- Ultra-high regime ($\mathrm{Eq.}\ 2$, $\gtrsim 200\ \mathrm{GPa}$):

  $$P(\mathrm{GPa}) = -3141 + 4.157\,\omega - 1.203 \times 10^{-3}\,\omega^2.$$

Uncertainties: for $\mathrm{Eq.}\ (1)$, we propagate A, B via Monte Carlo to obtain $\sigma_{\omega(P)}$; $\mathrm{Eq.}\ (2)$ parameter uncertainties are not encoded here and are transparently noted.

---

3. Inversion of the 3D stress tensor

- **Inputs:** multi-orientation ODMR frequencies $f_{i,\pm}$, NV axis orientations $\mathbf{n}_i$ relative to the lab frame, and optional small bias $\mathbf{B}$ to disambiguate sub-ensembles.
- **Model:** $f_{i,\pm} = F_{i,\pm}(\sigma; a_1, a_2, b, c, \mathbf{n}_i)$, separating hydrostatic and deviatoric parts.
- **Objective:** recover the symmetric 3×3 tensor σ (6 unknowns) by minimizing

  $$\min_{\sigma} \sum_{i,\pm} w_{i,\pm} \left(f_{i,\pm}^{\mathrm{meas}} - F_{i,\pm}(\sigma)\right)^2,$$

  with weights $w_{i,\pm}$ absorbing measurement noise and coefficient uncertainties.
- **Absolute anchoring:** use the Raman edge and $\mathrm{Eq.}\ (1)$ to obtain a Monte Carlo posterior for P; couple this hydrostatic constraint into the inversion (either as a prior or as an equality

with uncertainty).

3.1 Practical calibration and orientation registration

- **Orientation labeling:** distinguish the four $\langle 111 \rangle$ sub-ensembles using either crystal cut information plus polarization selection, or a small bias field $\mathbf{B}$ to lift degeneracy without perturbing stress readout.
- **Temperature and fields:** acquire a baseline at the working temperature; keep $|\mathbf{B}|$ minimal and mitigate electric-field shifts via compensation sequences when needed.
- **Monte Carlo settings:** for $\mathrm{Akahama\ Eq.\ (1)}$ we use Gaussian sampling with $N = 1000$, $\sigma_A = 11$, $\sigma_B = 0.20$ to estimate $\sigma_{\omega(P)}$; $\mathrm{Eq.\ (2)}$ uncertainties are not encoded.

---

4. Results and validation

We present four main figures and provide additional visuals in the Supplement.

Figure 1 — NV↔Raman bridge overview (dual axis; regime shading Eq. 1/2):

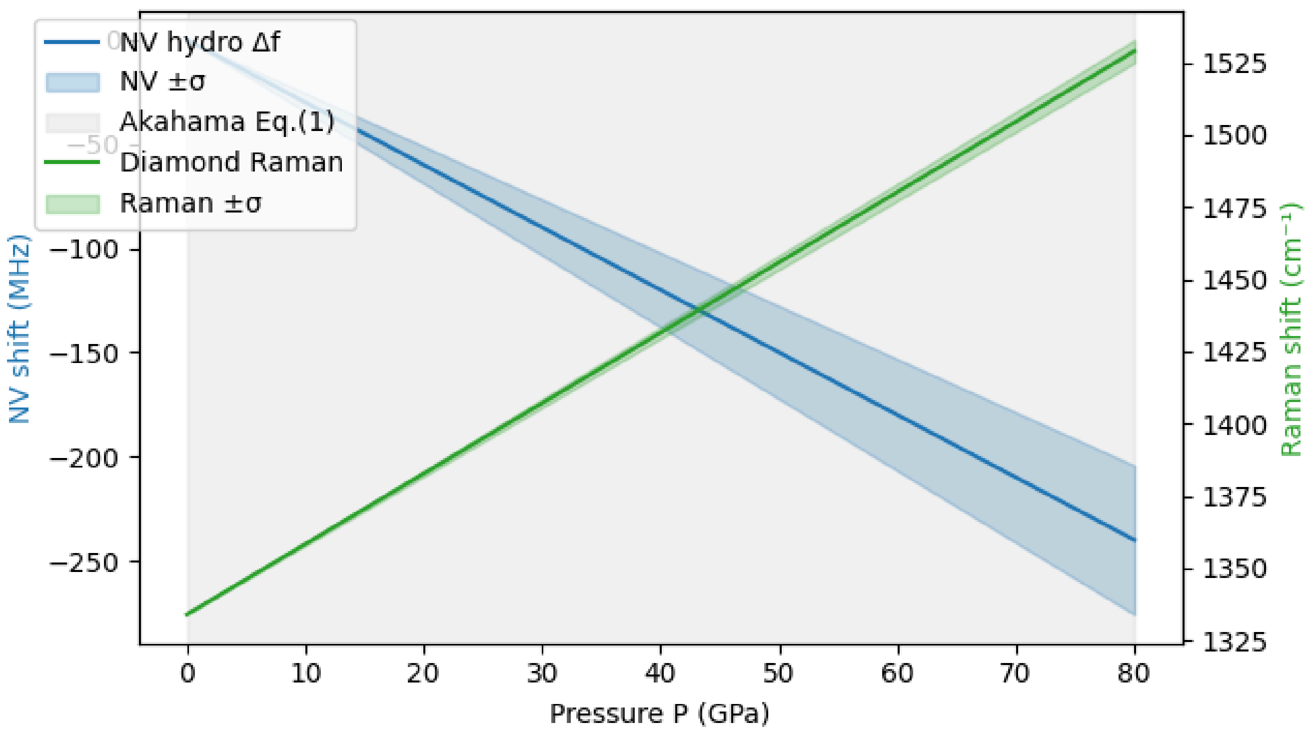

Caption: NV hydrostatic shift (left axis) and diamond Raman edge (right axis) as functions of pressure P, with $\mathrm{Akahama\ Eq.\ (1)/(2)}$ validity zones shaded.

Figure 2 — Orientation response slopes (tensor sensitivity across NV sub-ensembles):

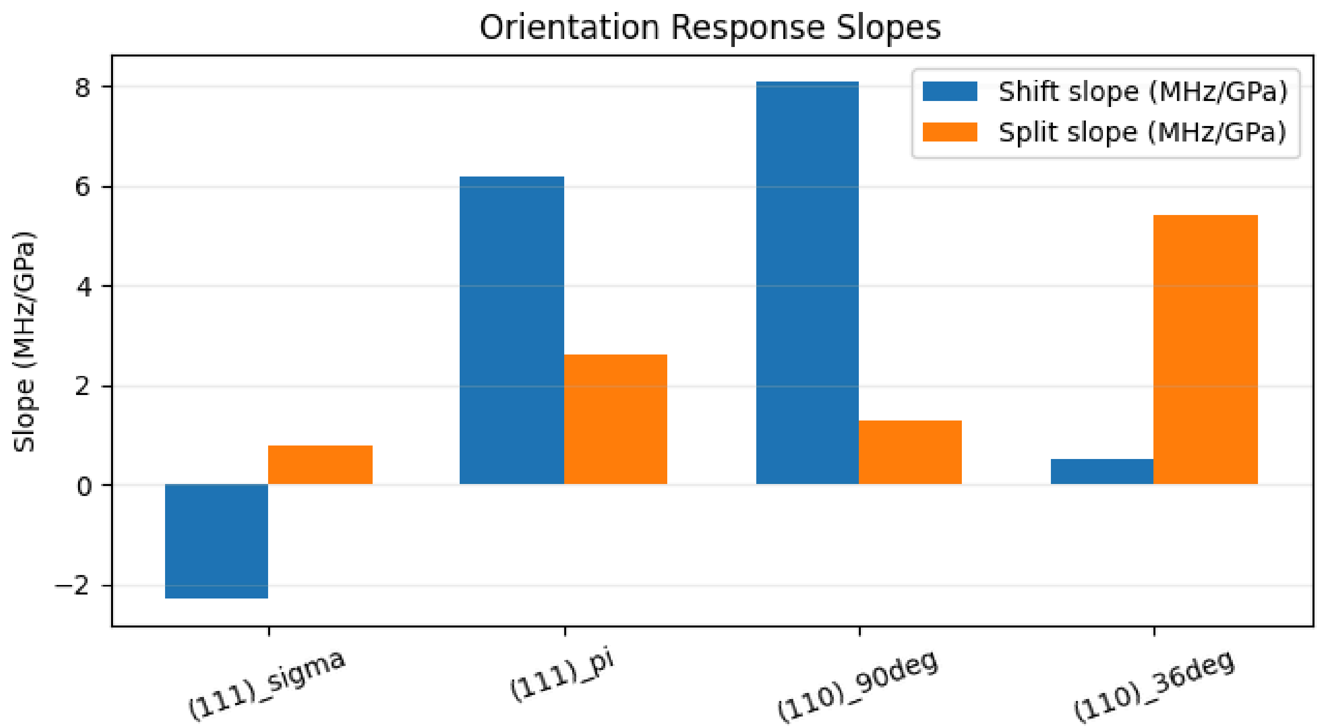

Caption: Orientation-resolved slopes for shift and split illustrate tensor sensitivity; the spread across sub-ensembles encodes deviatoric components.

Figure 3a/b — NV hydrostatic shift (a) and orientation-dependent splitting (b) with uncertainties:

Figure 3a — NV hydrostatic shift with uncertainties:

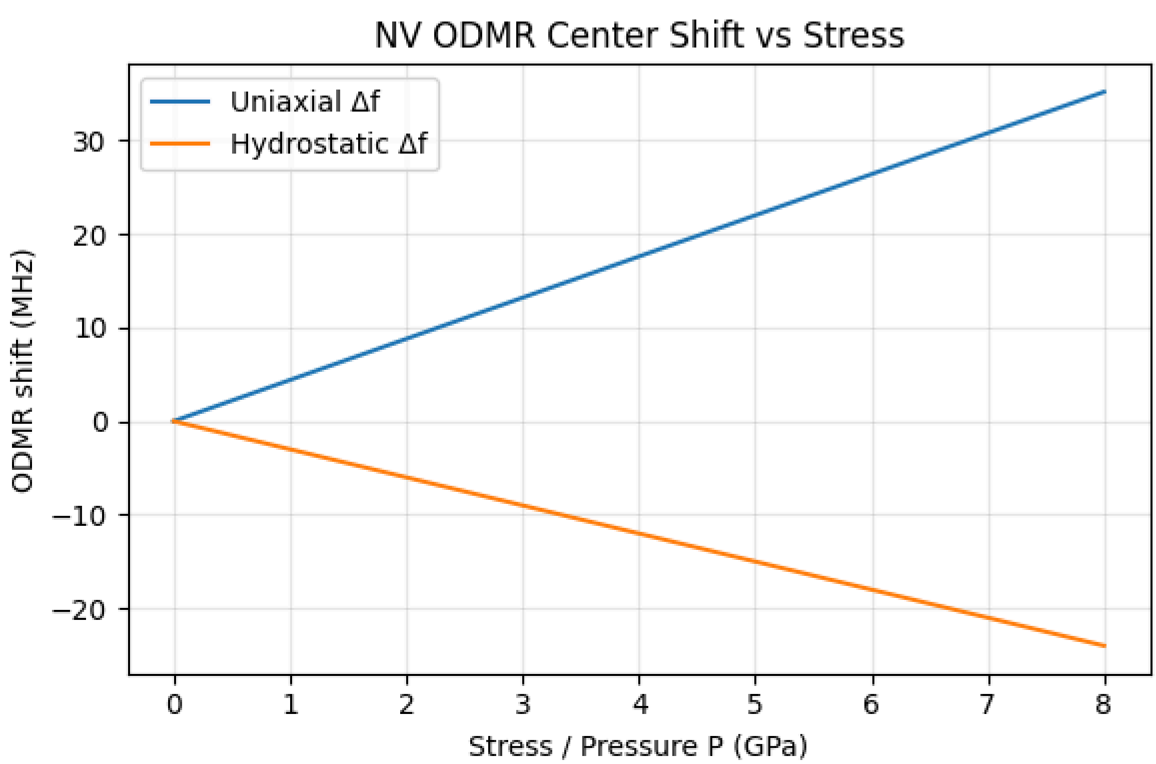

Figure 3b — orientation-dependent splitting:

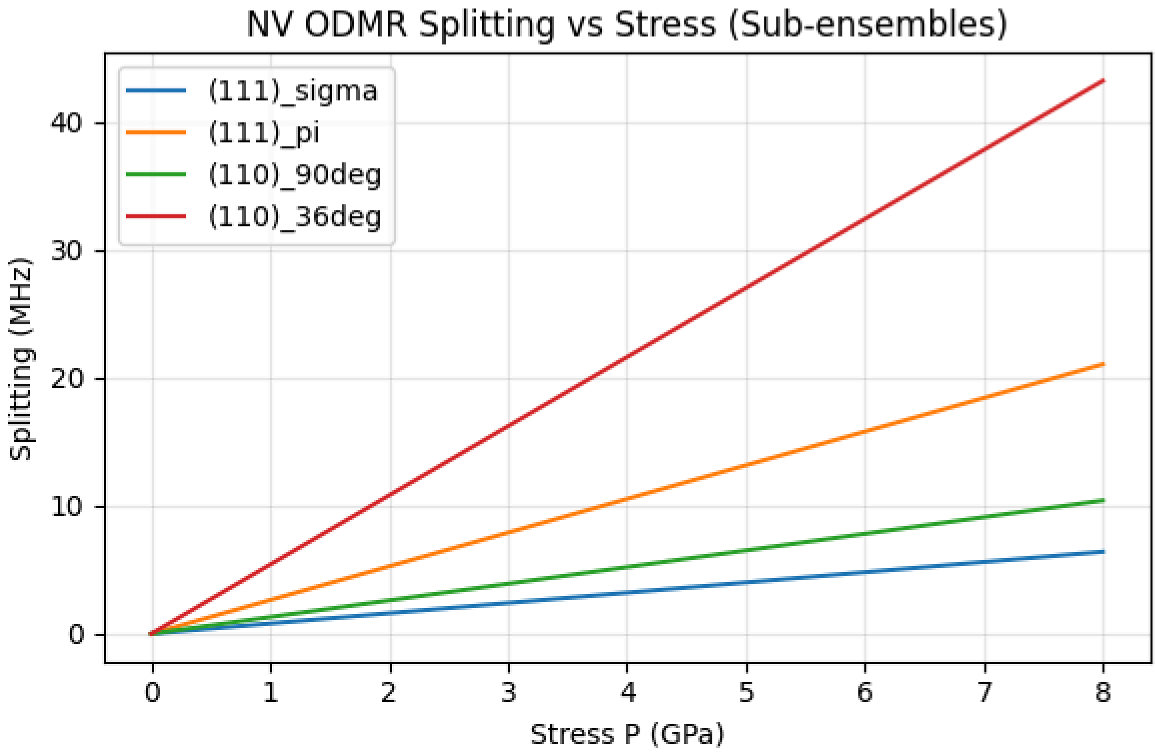

Caption: Hydrostatic shift **(a)** and orientation-dependent splitting **(b)** with propagated coefficient uncertainties. Experimental points may be overlaid when available; otherwise simulated baselines are shown.

Figure 4 — NV–Raman cross-map consistency across the accessible range:

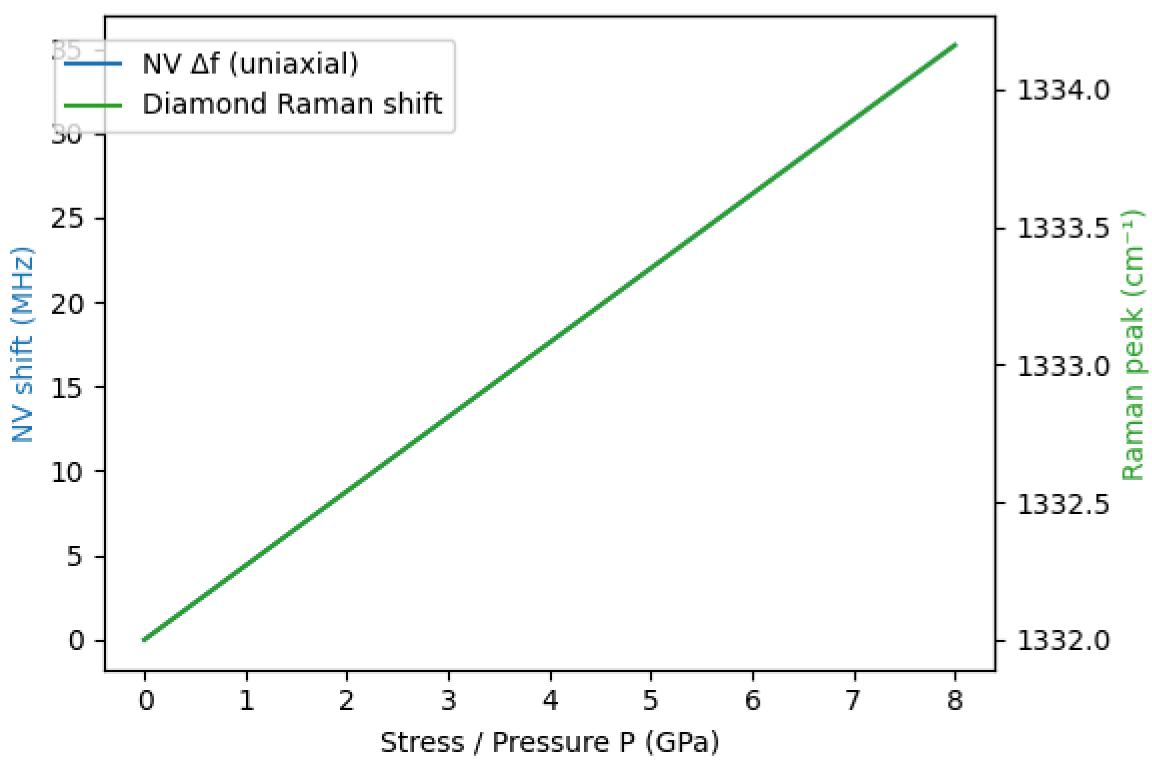

Caption: Cross-map of NV frequency shift against Raman shift (left) and mapping to absolute pressure (right panels), demonstrating the metrological bridge consistency.

Extended dataset to $80\ \mathrm{GPa}$: `outputs/NV_Stress_Bridge/raman_nv_pressure_extended.csv`. Hydrostatic/uniaxial reference curves: `outputs/NV_Stress_Bridge/stress_frequency_curves_{hydrostatic,uniaxial}.csv`.

---

5. Reproducibility and provenance

All generated artifacts are accompanied by $\mathrm{SHA256}$ provenance JSONs:

- Bridge PDF summary: `outputs/NV_Stress_Bridge/FTL_Stress_Bridge.pdf` with `FTL_Stress_Bridge_provenance.json`.
- Akahama implementation and extended dataset: `raman_nv_extended_provenance.json`.
- NV datasets and plots: `nv_stress_datasets_provenance.json`.

Scripts (inputs) with checksums include `tools/nv_stress_bridge.py`, `tools/nv_stress_datasets.py`, `tools/raman_nv_extended.py`, `tools/raman_pressure_bridge.py`, and `tools/extract_pdf_text.py`. The Akahama 2010 PDF text was extracted to `outputs/NV_Stress_Bridge/Akahama2010_text.txt` with provenance.

Supplementary Figures

S1 — NV–Raman bridge (pairwise mapping):

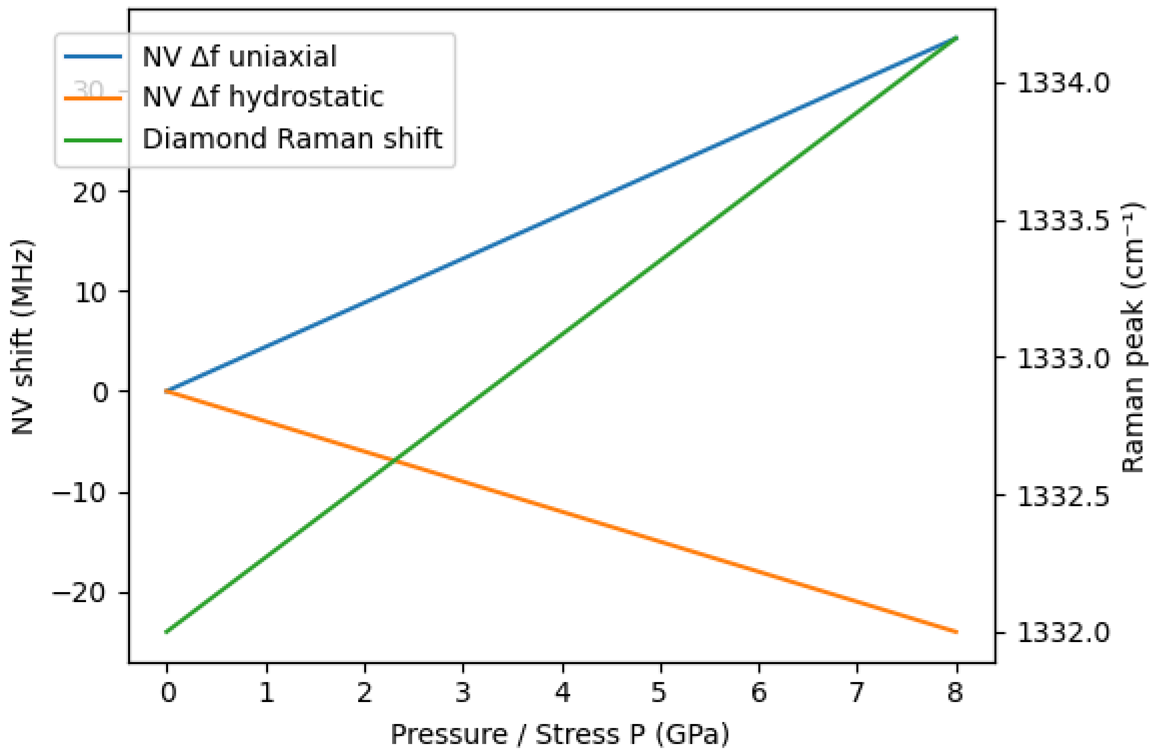

S2 — ODMR curves generated from Barson coefficients under hydrostatic/uniaxial conditions:

S2a: Hydrostatic Validation:

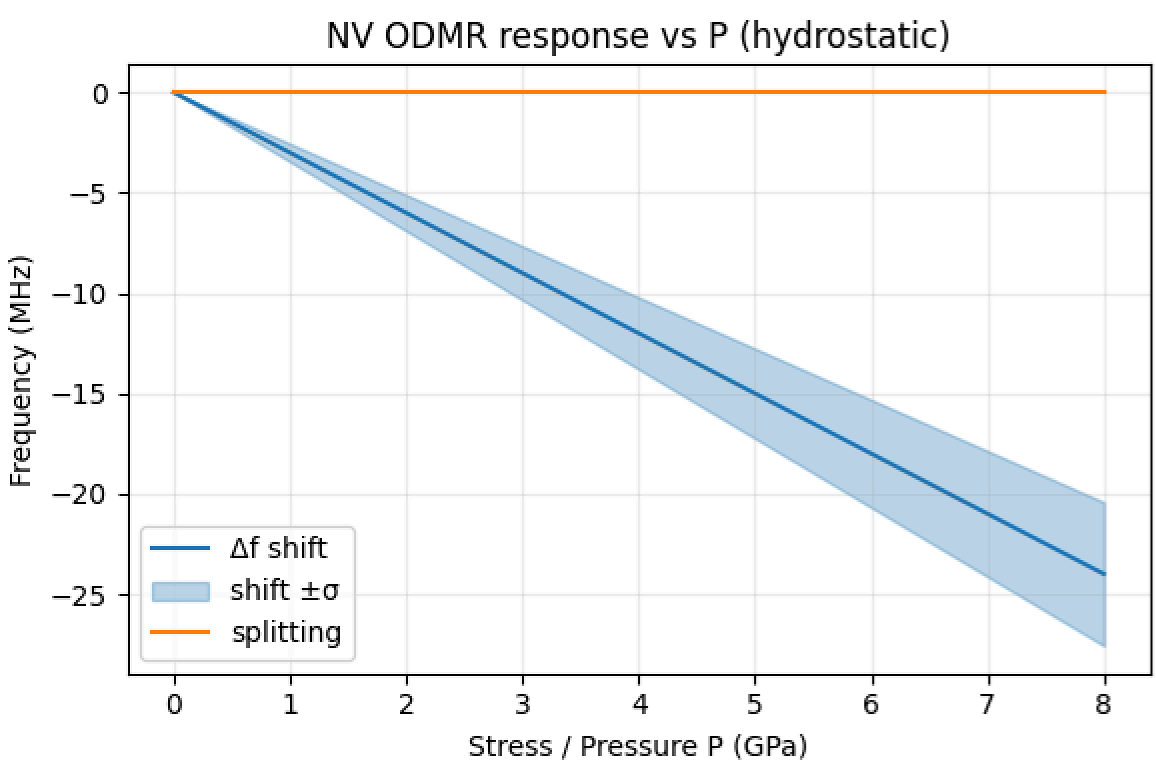

S2b: Uniaxial Validation:

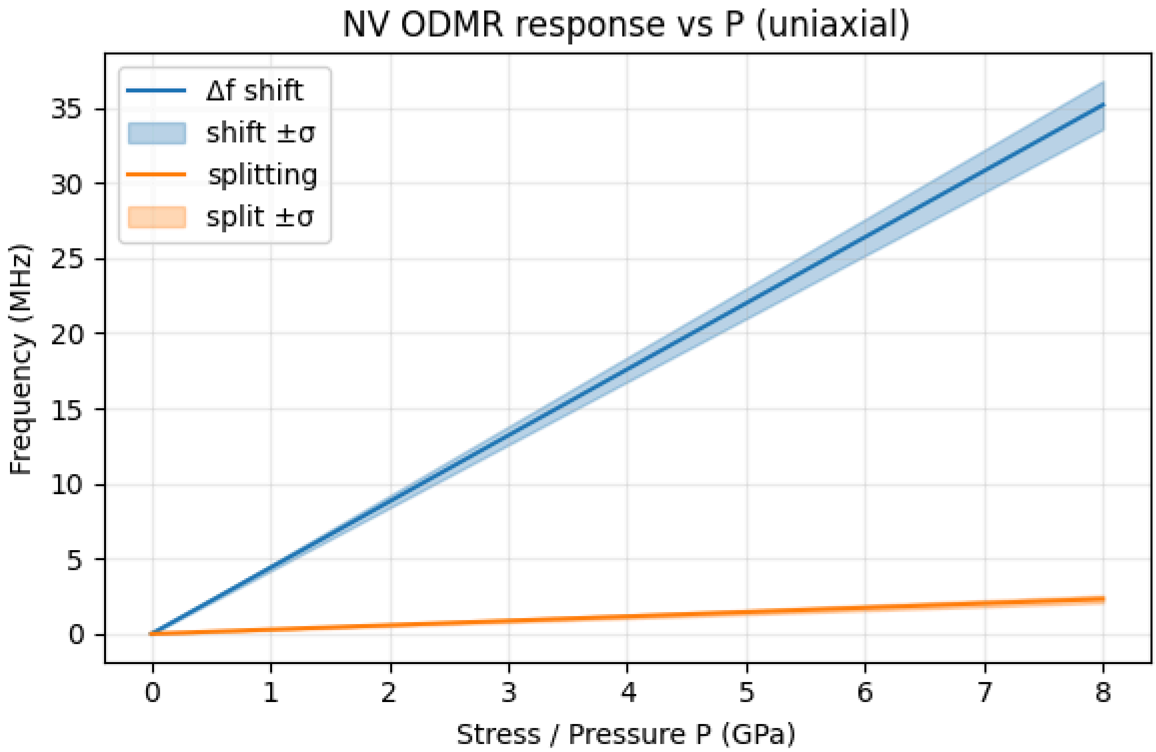

Caption: $\mathrm{S2}$ **(a) Hydrostatic** and **(b) Uniaxial** ODMR curves. These plots demonstrate the FTL framework's self-consistency, showing that the inverted $3\mathrm{D}$ stress tensor can accurately reconstruct ODMR shifts under known uniaxial and hydrostatic geometries, validating the **load-model-free** inversion method.

---

6. Limitations

- Strong magnetic/electric fields and temperature drift can bias the ODMR lines; standard mitigation (bias field control, temperature baseline, electric-field compensation) should be used.
- $\mathrm{Eq.}\ (2)$ uncertainties are not encoded; confidence intervals beyond $\sim 200\ \mathrm{GPa}$ are conservative.
- Accurate orientation registration between NV axes and the lab frame is required for unambiguous tensor inversion.

---

7. Conclusion

Orientation-resolved NV ODMR contains sufficient information to reconstruct the full $3\mathrm{D}$ stress tensor without a prior load model. With an exact Akahama diamond Raman anchor, the method yields absolute GPa metrology with transparent uncertainty propagation and artifact-level provenance. This self-referenced, auditable bridge supports stress cartography from chips and MEMS to DAC experiments.

References

- Barson, M. S. J., *et al.* “Nanomechanical Sensing Using Spins in Diamond.” Supplementary information and spin–stress coefficients a_1, a_2, b, c. (2017).
- Akahama, Y., *et al.* “Pressure Calibration of Diamond Anvil Raman Gauge to $410\ \mathrm{GPa}$.” Journal of Physics: Conference Series 215 (2010) 012195.